

DWT Power Spectrum of the Two-Degree Field Galaxy Redshift Survey *

Yan-Chuan Cai^{1,2}, Jun Pan¹, Yong-Heng Zhao², Long-Long Feng¹ and Li-Zhi Fang³

¹ Purple Mountain Observatory, Chinese Academy of Sciences, Nanjing 210008; y.c.cai@durham.ac.uk

² National Astronomical Observatories, Chinese Academy of Sciences, Beijing 100012

³ Department of Physics, University of Arizona, Tucson, AZ 85721, US

Received 2007 August 5; accepted 2007 November 5

Abstract The power spectrum of the two-degree Field Galaxy Redshift Survey (2dFGRS) sample is estimated with the discrete wavelet transform (DWT) method. The DWT power spectra within $0.035 < k < 2.2 h \text{ Mpc}^{-1}$ are measured for three volume-limited samples defined in consecutive absolute magnitude bins $-19 \sim -18$, $-20 \sim -19$ and $-21 \sim -20$. We show that the DWT power spectrum can effectively distinguish Λ CDM models of $\sigma_8 = 0.84$ and $\sigma_8 = 0.74$. We adopt maximum likelihood method to perform three-parameter fitting of the bias parameter b , pairwise velocity dispersion σ_{pv} and redshift distortion parameter $\beta = \Omega_m^{0.6}/b$ to the measured DWT power spectrum. The fitting results state that in a $\sigma_8 = 0.84$ universe the best-fit values of Ω_m given by the three samples are mutually consistent within the range $0.28 \sim 0.36$, and the best fitted values of σ_{pv} are 398_{-27}^{+35} , 475_{-29}^{+37} and $550 \pm 20 \text{ km s}^{-1}$ for the three samples, respectively. In the model of $\sigma_8 = 0.74$, our three samples give very different values of Ω_m . We repeated the fitting using the empirical formula of redshift distortion. The result of the model of low σ_8 is still poor, especially, one of the best-fit values of σ_{pv} is as large as 10^3 km s^{-1} . We also repeated our fitting by incorporating a scale-dependent galaxy bias. This gave a slightly lower value of Ω_m . Differences between the models of $\sigma_8 = 0.84$ and $\sigma_8 = 0.74$ still exist in the fitting results. The power spectrum of 2dFGRS seems to disfavor models with low amplitude of density fluctuations if the bias parameter is assumed to be scale independent. For the fitting value of Ω_m to be consistent with that given by WMAP3, strong scale dependence of the bias parameters is needed.

Key words: methods: data analysis — methods: statistical — (cosmology:) cosmological parameters —(cosmology:) large-scale structure of universe

1 INTRODUCTION

The present clumpy structures indicated by galaxies on large scales are evolved from very small density fluctuations in the early era of the universe. The amplitude of the fluctuation is fundamental to the understanding of structure formation. A remarkable success of modern cosmology is that the amplitude of mass fluctuations detected by the anisotropy of cosmic microwave background radiation is in excellent agreement with the analysis of the galaxy clustering at low redshifts. Recently, the released WMAP third year data (WMAP3) refine most results of the cosmological parameters given by the WMAP 1st year data. However, the fluctuation amplitude smoothed in a spherical top hat window of radius of $8h^{-1} \text{ Mpc}$ is found as small as $\sigma_8 = 0.74_{-0.06}^{+0.05}$ (Spergel et al. 2007), which is significantly lower than the $\sigma_8 = 0.84 \pm 0.04$ of the WMAP 1st year data. The new result of σ_8 is a challenge to the cosmological parameter determinations

* Supported by the National Natural Science Foundation of China.

from samples of galaxies and galaxy clusters, most of which yield $\sigma_8 \simeq 0.9 - 1$ if the matter content of the universe $\Omega_m \leq 0.3$ (e.g. Reiprich & Böhringer 2002; Hoekstra et al. 2002; Refregier et al. 2002; Van Waerbeke et al. 2002; Bacon et al. 2003; Bahcall & Bode 2003; Seljak et al. 2005; Viel & Haehnelt 2006).

This problem motivated us to revisit the constraints on σ_8 given by the power spectrum of the sample of two-degree Field Galaxy Redshift Survey (2dFGRS). The final released spectroscopic catalog of the 2dFGRS contains 221414 galaxies with good redshift quality $Q \geq 3$ and covers approximately 1800 square degrees of the sky. It is a good sample for studying the fluctuations of cosmic mass field on large scales in the linear regime as well as on scales in nonlinear range. Moreover, the 2dFGRS team has made detailed analysis of the Fourier power spectrum, the two point correlation functions and the relevant cosmological parameter fitting (Percival et al. 2001; Norberg et al. 2001; Peacock et al. 2001; Norberg et al. 2002; Hawkins et al. 2003; Percival et al. 2004; Cole et al. 2005). They found that $\Omega_m \sim 0.3$ or less (Peacock et al. 2001; Cole et al. 2005), and the best fit value of σ_8 is ~ 0.95 if one takes $\Omega_m \sim 0.3$ (Peacock et al. 2001), which is substantially different from WMAP3.

In the linear regime σ_8 only controls the overall amplitude of the power spectrum, and it is degenerated with the linear bias parameter b . Power spectrum on small scales is more effective to constrain σ_8 than on large scales since the nonlinearity of the power spectrum is directly reflected by the value of σ_8 . Most measurements of the 2dFGRS power spectrum are on scales of $k < 1h \text{ Mpc}^{-1}$ while cosmological parameter estimation is performed on scale of $k < \sim 0.2h \text{ Mpc}^{-1}$ (Peacock et al. 2001; Percival et al. 2001; Tegmark et al. 2002; Cole et al. 2005). With the estimator based on the discrete wavelet transformation (DWT) (Yang et al. 2001a,b, 2002) we are to analyse the power spectrum of the 2dFGRS sample on scales down to $k \simeq 2h \text{ Mpc}^{-1}$. In this scale range, the redshift distortion of DWT diagonal mode power spectrum can be easily approximated and the aliasing effect is exactly eliminated by the DWT algorithm (Fang & Feng 2000).

This paper is organized as follows. In Section 2, the DWT power spectrum estimator is introduced. Section 3 describes the construction of samples. Section 4 deals with robustness and accuracy tests on the DWT power spectrum estimator. Section 5 lists our fitting results. Our conclusions are stated in Section 6. Throughout this paper, we take the Hubble constant to be $h = 0.7$.

2 DWT POWER SPECTRUM ESTIMATOR

The method of measuring galaxy power spectrum with multi-resolution analysis of discrete wavelet transformation has been developed in the last decade (e.g. Pando & Fang 1995, 1996; Fang & Feng 2000; Yang et al. 2001b, 2002; Zhan & Fang 2003). A brief summary of the method is given here, more details can be found in the Appendix.

2.1 DWT Power Spectrum

The observed galaxy number density distribution is

$$n_g(\mathbf{x}) = \sum_{m=1}^{N_g} w_m \delta^D(\mathbf{x} - \mathbf{x}_m), \quad (1)$$

where N_g is the total number of galaxies, $\mathbf{x} = (x_1, x_2, x_3)$ is the 3-dimensional position vector, \mathbf{x}_m the position of the m^{th} galaxy, w_m its weight, and δ^D the 3-D Dirac δ function. For an observed sample, $n_g(\mathbf{x})$ can be regarded as a realization of a Poisson point process of intensity $n(\mathbf{x}) = \bar{n}_g(\mathbf{x})[1 + \delta(\mathbf{x})]$, where $\bar{n}_g(\mathbf{x})$ is the selection function, and $\delta(\mathbf{x})$ is the density contrast.

In terms of DWT decomposition, the galaxy field is described equivalently by variables defined as

$$\bar{\epsilon}_{\mathbf{j}, \mathbf{l}} = \int \delta_g(\mathbf{x}) \psi_{\mathbf{j}, \mathbf{l}}(\mathbf{x}) d\mathbf{x}, \quad (2)$$

where $\delta_g(\mathbf{x}) = [n_g(\mathbf{x})/\bar{n}_g(\mathbf{x})] - 1$, $\psi_{\mathbf{j}, \mathbf{l}}(\mathbf{x})$ the basis of the DWT decomposition, where index $\mathbf{j} = (j_1, j_2, j_3)$ stands for the scale, and $\mathbf{l} = (l_1, l_2, l_3)$ for the position (see Appendix A). Since the orthogonal-normal bases $\psi_{\mathbf{j}, \mathbf{l}}(\mathbf{x})$ are complete, all second order statistical behavior of the field can be described by $\langle \bar{\epsilon}_{\mathbf{j}, \mathbf{l}} \bar{\epsilon}_{\mathbf{j}', \mathbf{l}'} \rangle$. The goal of power spectrum measurement is to estimate the power spectrum of the density

fluctuations $\delta(\mathbf{x}) = [n(\mathbf{x})/\bar{n}(\mathbf{x})] - 1$ from the observed realization $\delta_g(\mathbf{x}) = [n_g(\mathbf{x})/\bar{n}_g(\mathbf{x})] - 1$. It has been shown by Yang et al. (2001a) that the power of the fluctuations on modes with scale index \mathbf{j} can be estimated by

$$P_{\mathbf{j}} = I_{\mathbf{j}}^2 - N_{\mathbf{j}}, \quad (3)$$

in which

$$I_{\mathbf{j}}^2 = \frac{1}{2^{j_1+j_2+j_3}} \sum_{l_1=0}^{2^{j_1}-1} \sum_{l_2=0}^{2^{j_2}-1} \sum_{l_3=0}^{2^{j_3}-1} [\tilde{\epsilon}_{\mathbf{j}, \mathbf{l}}]^2, \quad (4)$$

and

$$N_{\mathbf{j}} = \frac{1}{2^{j_1+j_2+j_3}} \sum_{l_1=0}^{2^{j_1}-1} \sum_{l_2=0}^{2^{j_2}-1} \sum_{l_3=0}^{2^{j_3}-1} \int \frac{\psi_{\mathbf{j}, \mathbf{l}}^2(\mathbf{x})}{\bar{n}_g(\mathbf{x})} d\mathbf{x}. \quad (5)$$

The term $I_{\mathbf{j}}^2$ is the mean power of \mathbf{j} modes measured from the observed realization $n_g(\mathbf{x})$, and $N_{\mathbf{j}}$ is the power on \mathbf{j} modes due to the Poisson noise. For a volume-limited survey, the mean galaxy density \bar{n}_g is independent of the redshift. The Poisson noise power is thus simply $1/\bar{n}_g$. $P_{\mathbf{j}}$ is usually referred to as the DWT power spectrum.

The DWT power spectrum $P_{\mathbf{j}}$ is related to the Fourier spectrum $P(n_1, n_2, n_3)$ by

$$P_{\mathbf{j}} = \frac{1}{2^{j_1+j_2+j_3}} \sum_{n_1=-\infty}^{\infty} \sum_{n_2=-\infty}^{\infty} \sum_{n_3=-\infty}^{\infty} |\hat{\psi}(n_1/2^{j_1})\hat{\psi}(n_2/2^{j_2})\hat{\psi}(n_3/2^{j_3})|^2 P(n_1, n_2, n_3), \quad (6)$$

where $\hat{\psi}(n)$ is the Fourier transform of the basic wavelet $\psi(x)$. Since $|\hat{\psi}(n)|^2$ is a high pass filter in the wavenumber space, $P_{\mathbf{j}}$ is banded Fourier power spectrum. If the cosmic density field is isotropic, the Fourier power spectrum $P(n_1, n_2, n_3)$ depends only on $n = \sqrt{n_1^2 + n_2^2 + n_3^2}$. Equation (6) is exact for homogeneously random fields, either Gaussian or non-Gaussian.

2.2 DWT Algorithm of Redshift-distortion

The DWT power spectrum depends on the scale and shape of the DWT mode $\psi_{\mathbf{j}, \mathbf{l}}(\mathbf{x})$, which is sensitive to distortion of the shape of the field. It is necessary to establish the mapping from the redshift space to the real space. Details of the mapping are given in Appendix D. The mapping is attributed to bulk velocity and pairwise peculiar velocity. In the linear treatment of bulk velocity, the redshift-distorted DWT power spectrum, $P_{\mathbf{j}}^S$, is related to the real space power spectrum $P_{\mathbf{j}}$ by (Yang et al. 2002)

$$P_{\mathbf{j}}^S = b^2(1 + \beta S_{\mathbf{j}})^2 S_{\mathbf{j}}^{\text{PV}} P_{\mathbf{j}}, \quad (7)$$

in which $\beta = \Omega_m^{0.6}/b$, b is the linear bias parameter. In Equation (7) $S_{\mathbf{j}}$ is the linear redshift distortion factor. For a cubic box of $L_1 = L_2 = L_3 = L$,

$$S_{j_1, j_2, j_3} = \frac{1}{2^{j_1+j_2+j_3}} \sum_{n_1, n_2, n_3=-\infty}^{\infty} \frac{n_3^2}{n_1^2 + n_2^2 + n_3^2} \cdot |\hat{\psi}(n_1/2^{j_1})\hat{\psi}(n_2/2^{j_2})\hat{\psi}(n_3/2^{j_3})|^2. \quad (8)$$

For diagonal modes $j_1 = j_2 = j_3 = j$, $S_{j, j, j} = \frac{1}{3}$. The factor $S_{\mathbf{j}}^{\text{PV}}$ in Equation (7) is the pairwise velocity dispersion factor. In the plane-parallel approximation, if the direction j_3 is chosen to be the line of sight, i.e., the redshift distortion is approximated only in the direction of j_3 , we have $S_{\mathbf{j}}^{\text{PV}} = [s_{\mathbf{j}}^{\text{PV}}]^2$, with

$$s_{j_1, j_2, j_3}^{\text{PV}} = \frac{1}{2^{j_3}} \sum_{n_3=-\infty}^{\infty} |\hat{\psi}(n_3/2^{j_3})|^2 \exp[-\frac{\sigma_{\text{pv}}^2}{2} (\frac{2\pi n_3}{L})^2]. \quad (9)$$

We will always take the plane-parallel approximation form of Equation (7) for our fitting. Correspondingly, for the 2dF volume-limited samples, we also take the plane parallel approximation and

Table 1 Volume Limited Sub-samples of 2dFGRS

$M_{b_J} - 5 \log_{10} h$	z_{\min}	z_{\max}	d_{\min}	d_{\max}	$N_g^{\text{SGP}}/N_g^{\text{NGP}}$	$\bar{n}(10^{-3}h^3 \text{Mpc}^{-3})$
-19 ~ -18	0.0205	0.087	61.2	255.7	9737/7811	8.393
-20 ~ -19	0.0320	0.129	95.2	374.9	19122/14390	5.102
-21 ~ -20	0.0495	0.186	146.6	532.9	14734/10202	1.330

always take j_3 as the line of sight direction (or z direction in real space). Obviously, the factor $(1 + \beta S_j)^2$ corresponds to the linear redshift distortion, and S_j^{PV} is the nonlinear redshift distortion caused by the pairwise velocity dispersion. Although Equation (7) is given by the linear approximation of bulk velocity, N-body simulations indicate that the mapping of Equation (7) works well till scale $k \simeq 2h \text{Mpc}^{-1}$, also because P_j is weakly affected by non-linear clumps of the density field. In general, for non-volume limited samples, selection function shall be taken into account to model redshift distortion which brings in high order correction to Equation (7) (Yang et al. 2002).

3 SAMPLE CONSTRUCTION

Samples used in our analysis are constructed basically in the same way as in Pan & Szapudi (2005). We create volume limited samples from the 2dFGRS spectroscopic catalog of the final data release (Colless et al. 2003), which contains 221414 galaxies with good redshift quality $Q \geq 3$ (Colless et al. 2001). We exclude the ancillary random fields, and use only the two major contiguous slices: one near the South Galactic Pole (SGP) covering approximately $-37^\circ.5 < \delta < -22^\circ.5$, $21^{\text{h}}40^{\text{m}} < \alpha < 3^{\text{h}}40^{\text{m}}$, one around the North Galactic Pole (NGP) defined roughly by $-7^\circ.5 < \delta < 2^\circ.5$, $9^{\text{h}}50^{\text{m}} < \alpha < 14^{\text{h}}50^{\text{m}}$. In order to obtain maximum number of galaxies while keeping a uniform sampling rate to guarantee fairness of our statistics, we tried different values of completeness f (f is defined as the ratio of the number of galaxies with redshifts to the total number of galaxies contained in the parent catalog): fields with completeness less than the chosen value are excluded, and fields with higher degrees of completeness are diluted to match the sampling rate. We find $f = 0.738$ is the optimal value. The final parent samples are thus restricted to completeness $f > 0.738$, and to apparent photometric b_J band magnitudes fainter than $m_{b_J} = 15$ and brighter than a median value of ~ 19.3 , with some small variation specified by the masks (Colless et al. 2003).

Volume limited sub-samples were built from the parent sample by selecting galaxies in specified absolute magnitude ranges. The absolute magnitudes were calculated with the $k+e$ corrections given in Norberg et al. (2002). Our analysis focusses on the three sub-samples defined in absolute magnitude M_{b_J} bins of $-19 \sim -18$, $-20 \sim -19$ and $-21 \sim -20$. The basic parameters of the three volume limited samples of 2dFGRS are summarized in Table 1 which lists, in turn, the redshift range, $z_{\min}-z_{\max}$, the range of comoving distances $d_{\min}-d_{\max}$, numbers of SGP and NGP galaxies, and the mean densities \bar{n} . The comoving distances were calculated from the redshifts z in the Λ CDM universe with $\Omega_\Lambda = 0.7$ and $\Omega_m = 0.3$.

4 NUMERICAL TESTS OF THE DWT POWER SPECTRUM ESTIMATOR

In this section, we will test the DWT power spectrum estimator with Poisson samples and that from the N-body simulation. Nine realizations of Poisson samples of 256^3 particles each are produced in a box of sides $L = 239.5 h^{-1} \text{Mpc}$. All the measured DWT power spectra of these samples are plotted in the left panel of Figure 1. First, to test the stability of the DWT estimator we calculate the diagonal DWT power spectrum, $P_{j,j,j}$, for each realization, and then compute their mean $\bar{P}_{j,j,j} \cdot P_{j,j,j}/\bar{P}_{j,j,j}$, shown in the right panel of Figure 1. We can see that at $j \leq 2$ (i.e. scales larger than $119.75h^{-1} \text{Mpc}$), there are as large as 50% variances in the diagonal DWT power spectrum. Thus we will not use data points with $j \leq 2$. At small scales, or large j , the DWT estimator gives reliable results. This is because the aliasing effect is effectively suppressed in the DWT analysis Fang & Feng (2000).

Second, in order to test the geometric effect of samples on estimation of the power spectrum, we cut one of the Poisson samples into three sheet-like sub-samples of $60.0 \times 239.5 \times 239.5$, $20.0 \times 239.5 \times 239.5$, and $20.0 \times 60.0 \times 239.5 (h^{-1} \text{Mpc})^3$. Then, a fourth sub-sample is constructed from the $20.0 \times 239.5 \times 239.5 (h^{-1} \text{Mpc})^3$ sub-sample by cutting off three parallel cylinders with radii 5.0, 10.0 and $20.0 h^{-1} \text{Mpc}$,

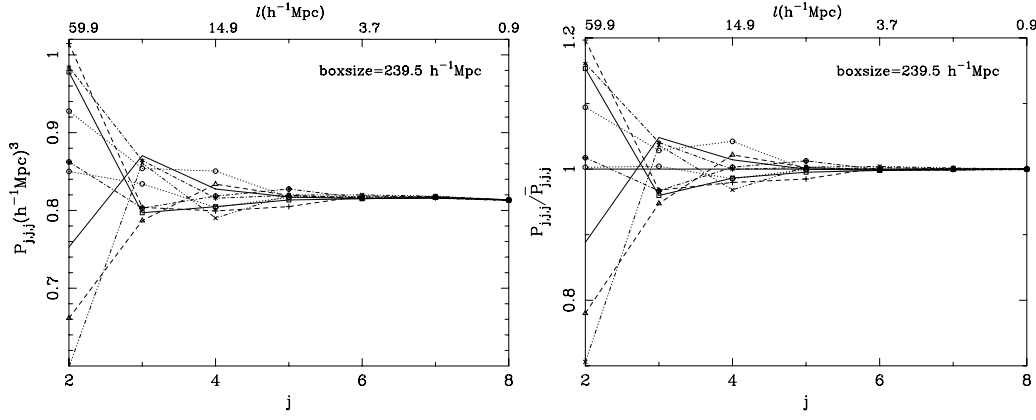


Fig. 1 *Left*: Diagonal DWT power spectra of nine realizations of Poisson samples. Each sample is generated in a box of size $239.5 h^{-1} \text{ Mpc}$ and 256^3 particles. The relation between j and the physical scale is $l = 239.5/2^j h^{-1} \text{ Mpc}$. *Right*: Ratios of diagonal DWT power spectra of nine realizations of Poisson samples to their mean spectrum.

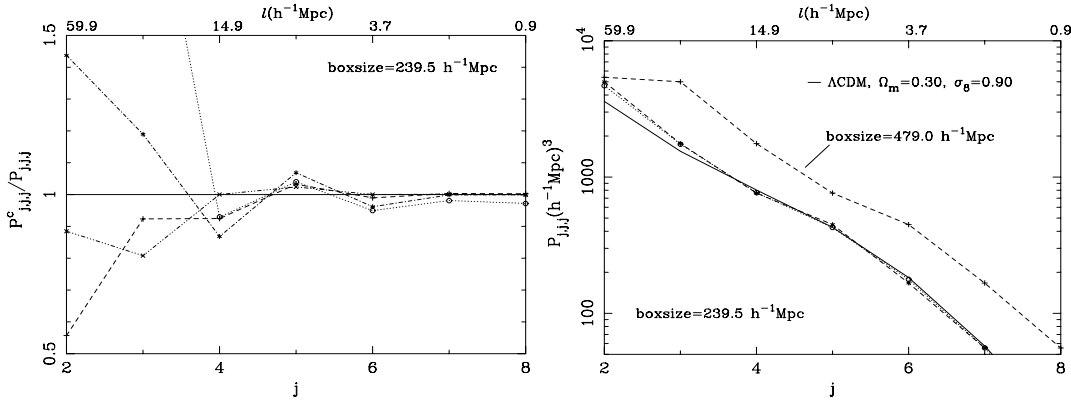


Fig. 2 *Left*: Ratios of DWT power spectra of cut Poisson sub-samples to the parent Poisson sample. The parent Poisson sample is generated in a box of size $239.5 h^{-1} \text{ Mpc}$, with 256^3 points. The sub-samples are defined in boxes of $60.0 \times 239.5 \times 239.5 h^{-1} \text{ Mpc}$ (dash-dot-dot line); $20.0 \times 239.5 \times 239.5 h^{-1} \text{ Mpc}$ (dash line); $20.0 \times 60.0 \times 239.5 h^{-1} \text{ Mpc}$ (dash-dot line); and $20.0 \times 60.0 \times 239.5 h^{-1} \text{ Mpc}$ with three cylinders chopped off (dot line). *Right*: DWT power spectrum of the Virgo simulation sample. The dash line on the right is measured with the size $479.0 h^{-1} \text{ Mpc}$ box. Shifting the right dash line by one unit along j -axis, we get the dash line on the left. The dot line is the power spectrum measured in the size $239.5 h^{-1} \text{ Mpc}$ box. The solid line is the nonlinear power spectrum from the formula of Smith et al. (2003) with $\Omega_m = 0.3$, $\Omega_\Lambda = 0.7$ and $\sigma_8 = 0.9$.

respectively. In the left panel of Figure 2, we plot the ratios of the DWT power spectra of each sub-sample to their parent random sample $P_{j,j,j}^c / P_{j,j,j}$. For $j = 2$ and 3 (or on the scale of $239.5/2 h^{-1} \text{ Mpc}$ and $239.5/2^2 h^{-1} \text{ Mpc}$), the scatters in those spectra can be larger than 50%, and the ratios are randomly distributed with variances of the order of unity. Actually, such significant scatters result from a small number of modes on $j \leq 3$. For $j > 3$, the differences between those spectra are negligible, the DWT power spectrum estimator is well independent of sample geometry on small scales.

Third, to test the reliability of the DWT power spectrum estimator, we measured the DWT power spectrum of the Virgo simulation under a ΛCDM cosmology with 256^3 particles in box of size $239.5 h^{-1} \text{ Mpc}$.

The right panel of Figure 2 compares the theoretical DWT power spectrum with that estimated from the simulation. The theoretical DWT power spectrum is calculated from Equation (6) with nonlinear power spectrum from the accurate fitting formula of Smith et al. (2003). Clearly, the theoretical spectrum and the measurements are in good agreement on scales smaller than $239.5/2^4 \simeq 15 h^{-1}$ Mpc. The test shows that the DWT power spectrum estimator can perfectly recover the original power spectrum on small scales.

For the fourth test, we measure the DWT spectrum of the Virgo sample in a cubic window of sides $479.0 h^{-1}$ Mpc, which is twice the size of the simulation box. Theoretically the power at scale j in the box of sides $479.0 h^{-1}$ Mpc corresponds to that at scale $j - 1$ in the box of sides $239.5 h^{-1}$ Mpc. It is clearly seen in the right panel of Figure 2 that the spectrum measured in the $479.0 h^{-1}$ Mpc box at j exactly equals to that measured in the $239.5 h^{-1}$ Mpc at $j - 1$. The DWT estimator is independent of the size of the window box. One can choose the size of box freely and put the sample in the box wherever one likes. Note that the difference of spectra at $j = 2, 3$ is greater than at other data points. Therefore, in the following analysis of the 2dFGRS catalogs, the first two data points in our spectra are discarded.

Finally, we test the DWT power spectrum estimator by mock galaxy catalogs. We created mock volume limited samples from the 22 mock galaxy catalogs which are extracted from the Hubble volume simulation¹. Details of the mock catalogs are in Cole et al. (1998). The set of mock samples used here is the LambdaCDM04. Real space galaxy positions are used. Therefore, no redshift distortion effect is expected. The 22 mock samples are filtered with the same selection criteria and masks as the real galaxy volume limited sub-samples. To achieve the largest possible volume, the NGP and the SGP regions are measured together in a window box of size $1403.0 h^{-1}$ Mpc. The size of the window is sufficient to cover all three volume limited sub-samples. For each of the three sub-samples, we obtain its mean DWT power spectrum of the mock galaxy samples by taking the average of 22 samples. Error bars are approximated by the $1-\sigma$ scattering, assuming the 22 mocks to be independent.

Shot noise is not directly calculated with Equation (5). Instead, we produce a number of Poisson samples with the same geometry as our samples. These Poisson samples have the numbers of galaxies as in the mock samples. The twenty-two Poisson samples for each sub-sample allow us to estimate the error bars for the shot noise subtraction.

Figure 3 (upper panel) shows the three mock DWT power spectra compared with the expected power spectrum. We can see that they agree very well, except at very large scales ($j = 2, 3$) or very small scales ($j = 8, 9$), where there is small discrepancy.

5 DWT POWER SPECTRUM OF 2DFGRS SAMPLES

5.1 The Diagonal DWT Power Spectrum

For the measurement of DWT power spectrum for the real 2dF galaxy sub-samples, we generally followed the same treatment as we did for the mock catalogues. We used a window box of size $1403.0 h^{-1}$ Mpc, combining the NGP and the SGP regions together. The filling factor of the sub-sample are 0.07%, 0.24% and 0.68%, respectively.

Error bars of the DWT power spectra were approximated by the $1-\sigma$ scattering of the 22 mock samples extracted from the Hubble volume simulation. Redshift space galaxy positions were used so as to be consistent with the real 2dF data. Shot noise was subtracted in the same way as we did for the mock catalogues.

In the bottom panel of Figure 3 we present the measured diagonal DWT power spectra of the three volume limited samples, together with two theoretical nonlinear spectra of flat Λ CDM model with parameters A) $\Omega_m = 0.3$, $\Omega_\Lambda = 0.7$ and $\sigma_8 = 0.84$ (Model A), and B) $\Omega_m = 0.24$, $\Omega_\Lambda = 0.76$ and $\sigma_8 = 0.74$ (Model B). The scale range is $0.035 < k < 2.2 h \text{ Mpc}^{-1}$.

5.2 Fitting of Redshift Distorted Power Spectrum

The differences between the power spectra of model predictions and the real data shown in the bottom panel of Figure 3 are mainly due to redshift distortion and bias. We adopted Equation (7) to fit the power spectrum of 2dFGRS samples with the nonlinear real space DWT power spectrum from Equation (6) and the formula of Smith et al. (2003). We first used the 22 mock samples to estimate the correlation between the powers of

¹ <http://star-www.dur.ac.uk/~cole/mocks/hubble.html>

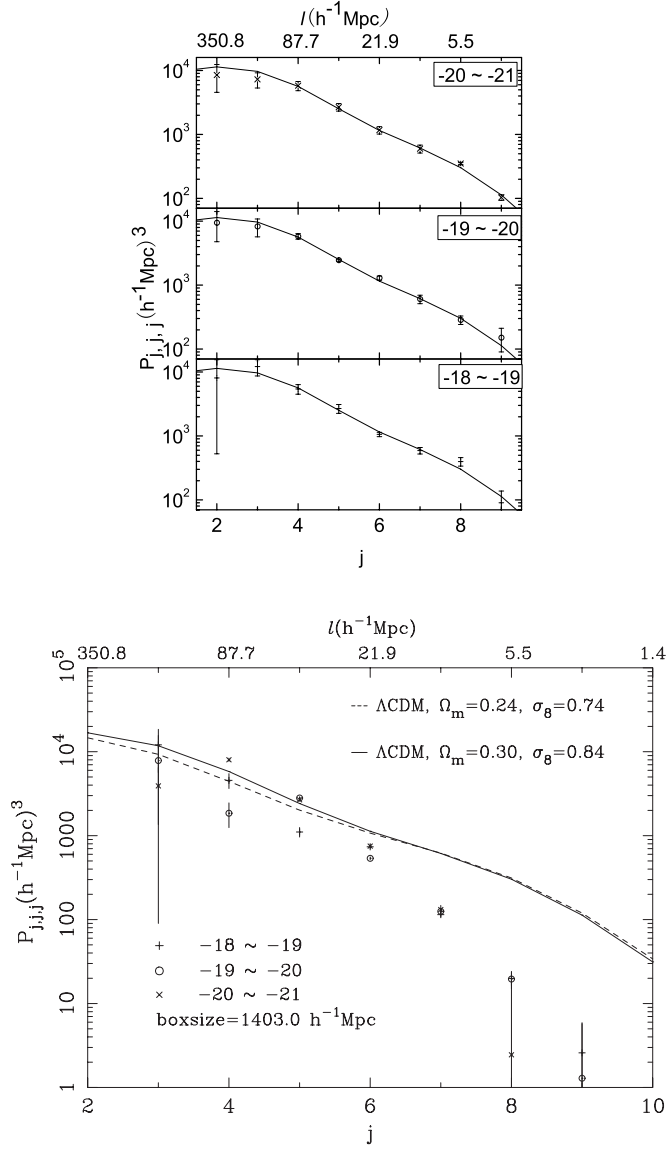


Fig. 3 Upper panel: Comparison of the expected DWT power spectrum and mock 2dF DWT power spectra. Solid line is the DWT power spectrum with $\Omega_m=0.3$, $\Omega_\Lambda=0.7$ and $\sigma_8=0.9$. The three panels are for the samples with limiting absolute magnitudes $-20 \sim -21$ (top); $-19 \sim -20$ (middle) and $-18 \sim -19$ (bottom). Bottom panel: DWT power spectrum of the 2dFGRS volume-limited samples and theoretical spectra. The size of the cubic box is $1403.0 h^{-1} \text{ Mpc}$. The relation between j and physical scale is $l = 1403.0/2^j h^{-1} \text{ Mpc}$. The power at large scales is suppressed by random motion of galaxies. Due to cosmic variance, the error bars at $j = 3$ are large. At $j = 9$, Poisson noise leads to the large error bars.

different DWT modes. We then constructed the covariance matrix

$$\tilde{C}_{jj'} = \frac{1}{N_{\text{sim}}} \sum_{I=1}^{N_{\text{sim}}} \Delta d_j^I \Delta d_{j'}^I, \quad (10)$$

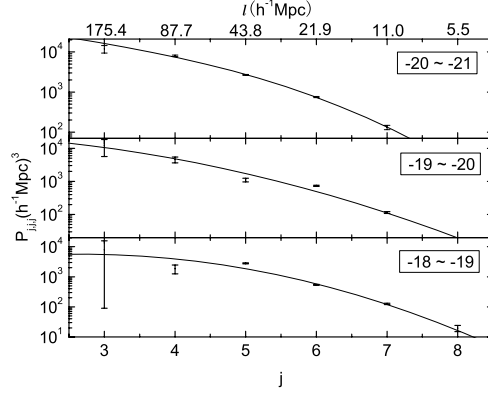


Fig. 4 DWT power spectra in redshift space of the Λ CDM model with $\sigma_8 = 0.84$. The parameters b , β , and σ_{pv} are given by our best fitting to the data points shown in the figure. The three panels are for sample with limiting absolute magnitudes $-20 \sim -21$ (top); $-19 \sim -20$ (middle) and $-18 \sim -19$ (bottom).

where $N_{\text{sim}} = 22$ and $\Delta d_j^I = d_j^I - \langle d_j \rangle$. The vector d^I consists of elements $d_j^I = P_{j,j}^I$ with $j = 3, \dots, 9$, $P_{j,j}^I$ is the power spectrum from the I -th simulation, and $\langle d_j \rangle$ is the mean. We found that the off-diagonal elements of the covariance matrices were always one order of magnitude smaller than the diagonal elements. Actually this is a typical feature in DWT analysis. The correlations between different modes are highly suppressed whether the field is Gaussian or non-Gaussian (Feng & Fang 2005). The quasi-diagonalizing of the correlation matrix in the DWT decomposition has been extensively used for data compression. By virtue of this property, we can compute χ^2 with the diagonal elements only, and we used the Chi-Square as our maximum likelihood estimator,

$$\chi^2 = \sum_{j=1}^N \frac{[P_j - P_j^S(a_1, a_2, a_3 \dots)]^2}{\sigma_j^2}, \quad (11)$$

in which P_j is the observed data and $P_j^S(a_1, a_2, a_3 \dots)$ is the redshift-distorted power of the model with parameters $(a_1, a_2, a_3 \dots)$. We take the Reduced-Chi-Square, which is defined as $\chi_{\text{d.o.f}}^2 = \chi^2 / (N - M)$ where $(N - M)$ is the degree of freedom, as our final results shown in the tables. For our fittings of DWT power spectrum, the degree of freedom would be $7 - 3 = 4$, unless otherwise specified.

We aim at detecting the influence of σ_8 on the power spectrum. Two fiducial Λ CDM models are considered here: A) $\sigma_8 = 0.84$, and B) $\sigma_8 = 0.74$. We took the linear bias parameters b , redshift distortion parameter β (or Ω_m) and pairwise velocity variance σ_{pv} as the fitting parameters. The other parameters of Models A and B are the same. The parameter space (b, β, σ_{pv}) is divided into a $20 \times 20 \times 20$ grid. The first run of fitting is performed on a very crude grid in broad parameter space to locate the region of best χ^2 . Then we decrease the volume of parameter space centered in this region with a finer grid to obtain the three dimensional probability distribution functions (PDF) of (b, β, σ_{pv}) . After integrating over two of the three parameters, we have the marginal PDF for the third parameter.

5.3 Results of Fitting

The best fitting power spectra of both models are very close to each other, so only those of model A are shown in Figure 4. The estimated parameters of models A and B are tabulated in Tables 2 and 3, respectively. As an example, the marginal PDFs of the parameters b, β, σ_{pv} for the sub-sample $-21 \sim -20$ are shown in Figure 5. Figure 6 gives the PDFs of Ω_m for all the three sub-samples.

In Table 2 we can see that the three sub-samples offer about the same estimates, with $\Omega_m \simeq 0.3$, and b increasing from 0.75 to $\simeq 1$ with the galaxy luminosity, in agreement with other researchers' analysis (Norberg et al. 2001; Pan & Szapudi 2005). The pairwise velocities obtained in the three samples are in

Table 2 Parameters estimated by fitting the 2dFGRS DWT power spectra with Eq. (7) to the Λ CDM model with $\sigma_8 = 0.84$.

$M_{b,J} - 5 \log_{10} h$	β / Ω_m	b	σ_{pv} (km s $^{-1}$)	$\chi^2/\text{d.o.f}$
-19 \sim -18	$0.66^{+0.06}_{-0.10} / 0.31^{+0.08}_{-0.12}$	$0.75^{+0.05}_{-0.06}$	398^{+36}_{-27}	8.87/4
-20 \sim -19	$0.62^{+0.07}_{-0.10} / 0.36^{+0.12}_{-0.14}$	$0.86^{+0.08}_{-0.07}$	475^{+37}_{-29}	16.19/4
-21 \sim -20	$0.43^{+0.02}_{-0.02} / 0.28^{+0.02}_{-0.02}$	$1.07^{+0.01}_{-0.01}$	550^{+20}_{-20}	4.06/4

Table 3 Parameters estimated by fitting the 2dFGRS DWT power spectra with Eq. (7) to the Λ CDM model of $\sigma_8 = 0.74$.

$M_{b,J} - 5 \log_{10} h$	β / Ω_m	b	σ_{pv} (km s $^{-1}$)	$\chi^2/\text{d.o.f}$
-19 \sim -18	$0.76^{+0.07}_{-0.09} / 0.41^{+0.10}_{-0.12}$	$0.77^{+0.05}_{-0.05}$	415^{+40}_{-26}	12.24/4
-20 \sim -19	$0.73^{+0.12}_{-0.10} / 0.46^{+0.20}_{-0.16}$	$0.86^{+0.09}_{-0.07}$	492^{+38}_{-40}	17.99/4
-21 \sim -20	$0.35^{+0.02}_{-0.02} / 0.28^{+0.02}_{-0.02}$	$1.19^{+0.01}_{-0.01}$	600^{+15}_{-15}	4.83/4

Table 4 Parameters estimated by fitting 2dFGRS DWT power spectra with Eq. (7) to the model of $\Omega_m = 0.24$ and $\Omega_\Lambda = 0.76$.

$M_{b,J} - 5 \log_{10} h$	σ_8	b	σ_{pv} km s $^{-1}$	$\chi^2/\text{d.o.f}$
-19 \sim -18	$0.43^{+0.20}_{-0.06}$	$0.99^{+0.20}_{-0.10}$	490^{+42}_{-40}	10.74/4
-20 \sim -19	$0.97^{+0.09}_{-0.06}$	$0.82^{+0.15}_{-0.13}$	445^{+45}_{-35}	16.83/4
-21 \sim -20	$0.94^{+0.04}_{-0.04}$	$0.99^{+0.09}_{-0.05}$	505^{+40}_{-35}	4.77/4

a reasonable range, and also increase with the galaxy luminosity. It appears that our analysis of model A ($\sigma_8 = 0.84$) is basically in good agreement with the previous works, and more importantly, that the DWT proves itself to be an effective tool for parameter estimation of galaxy samples.

The fitting to model B provides very different estimates of parameters. As seen in Table 3 and Figure 6, the values of Ω_m given by the three sub-samples are quite different from each other. The best values of Ω_m for the sub-samples of $-19 \sim -18$ and $-20 \sim -19$ are significantly larger than 0.3, which is in disagreement with most of the current measurements, at least at 1- σ level (Peacock et al. 2001; Tegmark et al. 2004). Only the sub-sample of $-21 \sim -20$ yields $\Omega_m \approx 0.3$.

In order to check the scale-dependence of our fitting results at small scales, we repeated the above fitting with data points at $j = 8$ excluded ($j = 8$ corresponds to a physical scale of $5.5 h^{-1}$ Mpc). Therefore, the smallest scale covered in the new fitting is $11.0 h^{-1}$ Mpc. We find that the central values of the fitting results are generally the same as before. For the value of Ω_m , the biggest difference is from the sub-sample $-20 \sim -21$. The central value is $\Omega_m = 0.26$, which is still less than 10%. For other sub-samples, the difference is normally less than 5%, or even negligible.

In fact, Percival et al. (2007) have shown by an analysis of SDSS DR5 galaxy power spectrum that there is discrepancy in the fitting results of Ω_m with different scales. Fitting on the scales $0.01 < k < 0.06 h \text{ Mpc}^{-1}$ gives $\Omega_m = 0.22 \pm 0.04$, which is smaller than $\Omega_m = 0.32 \pm 0.01$ for fitting on the scales $0.01 < k < 0.15 h \text{ Mpc}^{-1}$. Our analysis seems to give much less discrepancy in the fitting results on different scales. This smaller difference may be explained by the large error bars at $j = 8$, which make it contribute little to the χ^2 fitting. Moreover, note that our fittings with and without $j = 8$ corresponds to the largest k value being ~ 1 and ~ 2 , respectively, which is different from that given by Percival et al. (2007). Finally, our fitting formula, Equation (7), reflects both linear and non-linear effects. Therefore, fitting for linear and non-linear scales could have consistent results.

In order to place constraints from the 2dFGRS on σ_8 , we repeated the fitting procedure with σ_8 , b and σ_{pv} as fitting parameters, and $\Omega_m = 0.24$ as a fixed prior. Results are shown in Table 4. It is very clear that, the two sub-samples other than the $-19 \sim -18$ sub-sample both give a $\sigma_8 > 0.9$. Thus, a universe of $\sigma_8 = 0.74$ is not preferred by the DWT power spectrum of the 2dFGRS.

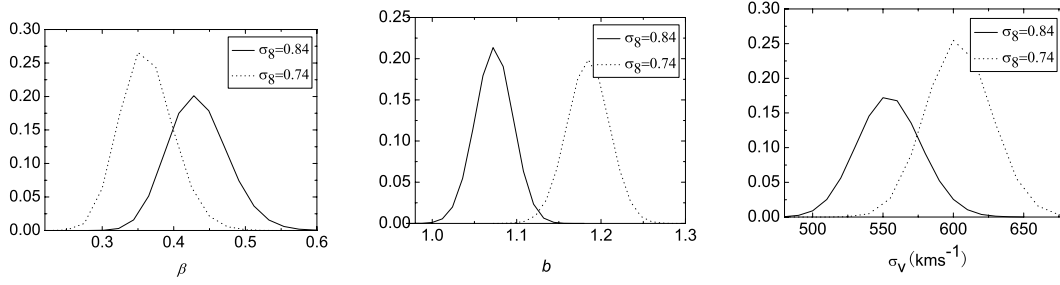


Fig. 5 Marginal distributions of the parameters b , β , and σ_{pv} in the fitting of DWT power spectrum to the 2dFGRS sample of $M_{b,j} \in (-20 \sim -21)$ with Eq. (7).

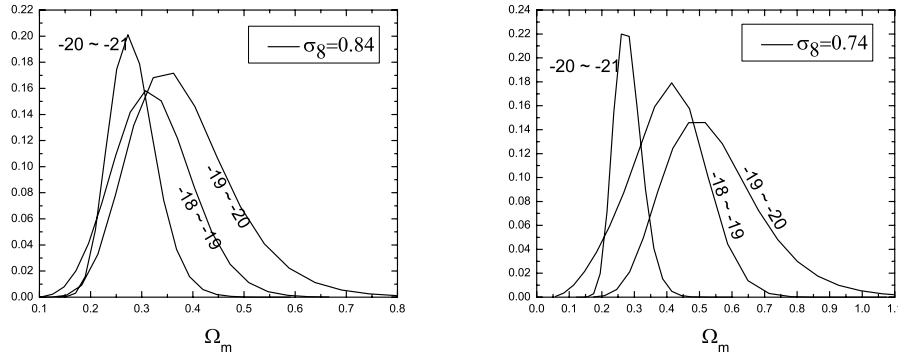


Fig. 6 Marginal distribution of Ω_m in the fitting of DWT power spectra with Eq. (7) to the 2dFGRS samples with $M_{b,j}$ in $-18 \sim 19$, $-19 \sim -20$ and $-20 \sim -21$.

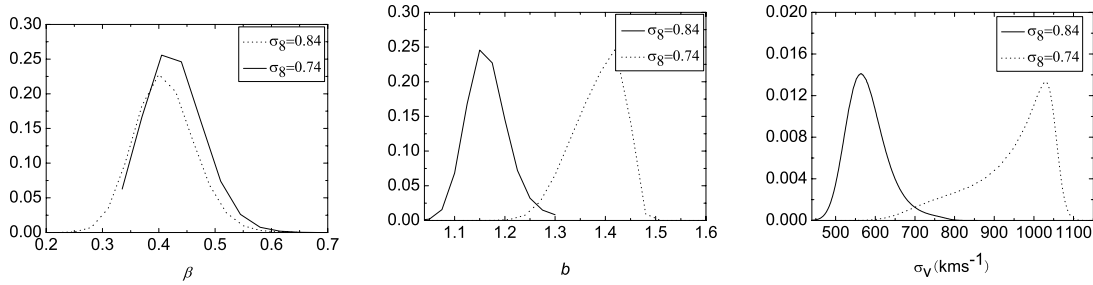


Fig. 7 Marginal distributions of β , b , σ_{pv} for the $-20 \sim -21$ sub-sample, with the empirical redshift distortion mapping formula of Eq. (12). Fitting with $\sigma_8 = 0.74$ gives a larger b and σ_{pv} than with $\sigma_8 = 0.84$.

5.4 Fitting with an Alternative Formula of Redshift Distortion

Empirically, the Fourier power spectrum $P^S(k)$ in redshift space is related to that in real space by Peacock & Dodds (1994)

$$P^S(k) = b^2 P(k) G(y, \beta), \quad (12)$$

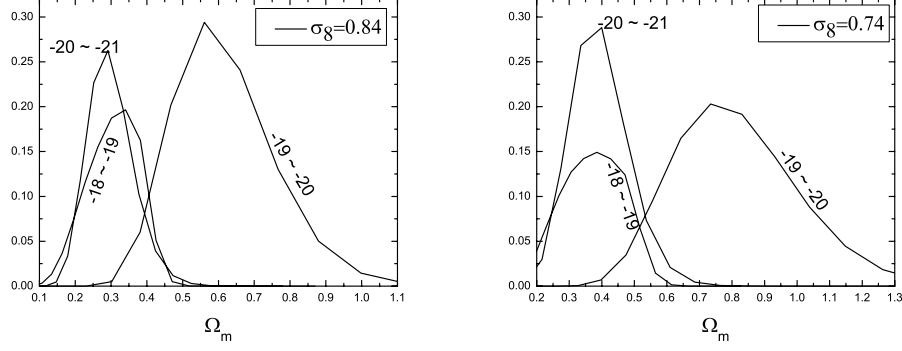


Fig. 8 Marginal distribution of Ω_m in the three-parameter fitting with Eq. (12). For all the sub-samples, fitting with the lower σ_8 gives a larger value of Ω_m .

Table 5 Best parameters from fitting DWT power spectra to Λ CDM model with $\sigma_8 = 0.84$ and Eq. (12).

$M_{b_J} - 5 \log_{10} h$	β / Ω_m	b	$\sigma_{\text{pv}} \text{ (km s}^{-1}\text{)}$	$\chi^2/\text{d.o.f}$
-19 ~ -18	$0.77^{+0.08}_{-0.17} / 0.34^{+0.15}_{-0.20}$	$0.69^{+0.12}_{-0.09}$	315^{+68}_{-44}	10.91/4
-20 ~ -19	$0.73^{+0.06}_{-0.12} / 0.56^{+0.14}_{-0.22}$	$0.97^{+0.08}_{-0.07}$	578^{+50}_{-40}	8.46/4
-21 ~ -20	$0.41^{+0.07}_{-0.03} / 0.28^{+0.10}_{-0.05}$	$1.15^{+0.05}_{-0.03}$	548^{+68}_{-26}	4.96/4

Table 6 Best parameters from fitting DWT power spectra to Λ CDM model with $\sigma_8 = 0.74$ and Eq. (12).

$M_{b_J} - 5 \log_{10} h$	β / Ω_m	b	$\sigma_{\text{pv}} \text{ (km s}^{-1}\text{)}$	$\chi^2/\text{d.o.f}$
-19 ~ -18	$0.76^{+0.08}_{-0.17} / 0.38^{+0.15}_{-0.20}$	$0.74^{+0.10}_{-0.07}$	336^{+57}_{-41}	10.61/4
-20 ~ -19	$0.73^{+0.06}_{-0.12} / 0.73^{+0.19}_{-0.27}$	$1.13^{+0.09}_{-0.07}$	682^{+43}_{-41}	8.26/4
-21 ~ -20	$0.40^{+0.06}_{-0.03} / 0.39^{+0.11}_{-0.07}$	$1.42^{+0.03}_{-0.06}$	1014^{+51}_{-113}	4.89/4

Table 7 Best parameters $\sigma_8, b, \sigma_{\text{pv}}$ from fitting DWT power spectra to Λ CDM model with $\Omega_m = 0.24, \Omega_\Lambda = 0.76$, and Eq. (12).

$M_{b_J} - 5 \log_{10} h$	σ_8	b	$\sigma_{\text{pv}} \text{ km s}^{-1}$	$\chi^2/\text{d.o.f}$
-19 ~ -18	$0.80^{+0.14}_{-0.08}$	$0.73^{+0.21}_{-0.12}$	325^{+66}_{-50}	17.00/4
-20 ~ -19	$0.93^{+0.10}_{-0.07}$	$0.91^{+0.15}_{-0.14}$	470^{+57}_{-51}	15.62/4
-21 ~ -20	$0.98^{+0.04}_{-0.04}$	$0.97^{+0.05}_{-0.04}$	412^{+50}_{-43}	7.16/4

in which $y^2 = k^2 \sigma_{\text{pv}}^2$, and the function G is

$$G(y, \beta) = \frac{\sqrt{\pi} \operatorname{erf}(y)}{8 y^5} [3\beta^2 + 4\beta y^2 + 4y^4] - \frac{\exp(-y^2)}{4y^4} [\beta^2(3 + 2y^2) + 4\beta y^2]. \quad (13)$$

Substituting Equation (6) into Equation (12) yields

$$P_{j,j,j}^S(b, \beta, \sigma_{\text{pv}}) = b^2 P_{j,j,j} G[y(j), \beta], \quad (14)$$

where $y(j) = k^2(j) \sigma_{\text{pv}}^2$ and $k(j)$ is given by Equation (B12).

Following the same procedure as in Section 5.2, we carried out a three-parameter ($b, \beta, \sigma_{\text{pv}}$) fitting with Equation (14). The fitting results of model A and model B are given in Tables 5 and 6, respectively. The

Table 8 Parameters estimated by fitting 2dFGRS DWT power spectra with Eq. (17) to Λ CDM model of $\sigma_8 = 0.84$.

$M_{b_J} - 5 \log_{10} h$	Ω_m	b_o	$\sigma_{\text{pv}} \text{ (km s}^{-1}\text{)}$	$\chi^2/\text{d.o.f}$
-19 \sim -18	$0.28^{+0.05}_{-0.06}$	$0.41^{+0.02}_{-0.02}$	480^{+35}_{-25}	16.37/4
-20 \sim -19	$0.31^{+0.06}_{-0.05}$	$0.43^{+0.02}_{-0.02}$	520^{+40}_{-30}	21.98/4
-21 \sim -20	$0.25^{+0.02}_{-0.02}$	$0.52^{+0.01}_{-0.01}$	587^{+18}_{-18}	6.77/4

Table 9 Parameters estimated by fitting 2dFGRS DWT power spectra with Eq. (17) to Λ CDM model of $\sigma_8 = 0.74$.

$M_{b_J} - 5 \log_{10} h$	Ω_m	b_o	$\sigma_{\text{pv}} \text{ (km s}^{-1}\text{)}$	$\chi^2/\text{d.o.f}$
-19 \sim -18	$0.39^{+0.07}_{-0.08}$	$0.44^{+0.02}_{-0.02}$	495^{+30}_{-25}	14.98/4
-20 \sim -19	$0.38^{+0.10}_{-0.09}$	$0.43^{+0.02}_{-0.02}$	525^{+45}_{-30}	20.25/4
-21 \sim -20	$0.23^{+0.02}_{-0.02}$	$0.58^{+0.02}_{-0.02}$	650^{+20}_{-20}	8.92/4

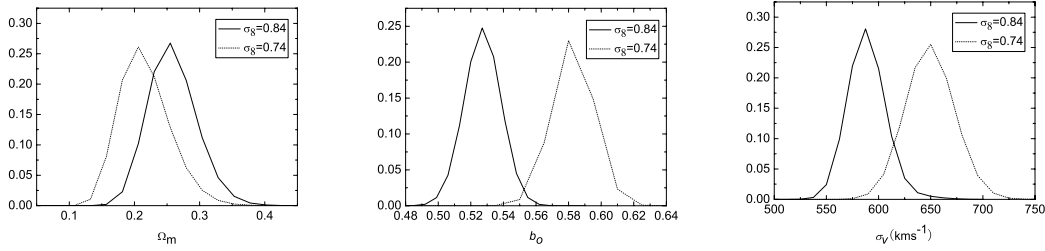


Fig. 9 Marginal distribution of parameters $\Omega_m, b_o, \sigma_{\text{pv}}$ for the $-20 \sim -21$ sub-sample, with the DWT redshift distortion mapping formula of Eq. (17), incorporating the scale dependence bias model.

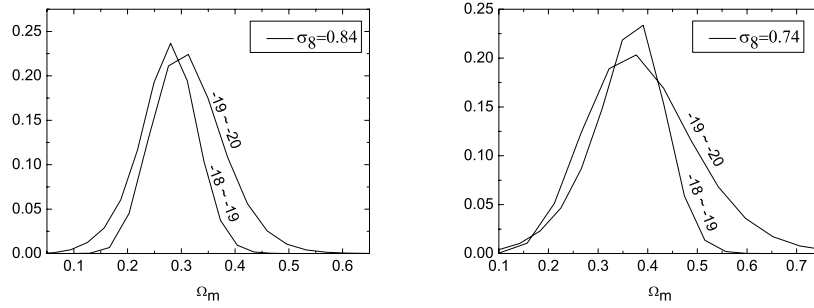


Fig. 10 Marginal distribution of Ω_m in the three-parameter fitting with Eq. (17). For the two sub-samples shown, fitting with the lower σ_8 gives a larger value of Ω_m .

PDFs of the three parameters $b, \beta, \sigma_{\text{pv}}$ for the sub-sample of $-21 \sim -20$ are plotted in Figure 7, and the PDFs of Ω_m for all the three sub-samples are in Figure 8. Figure 7 shows that the models A and B have very different PDFs of σ_{pv} : the PDF in model B is highly skewed and very broad while the PDF in model A is close to a Gaussian.

The result of model A shown in Table 5 is roughly the same as that in Table 2. The sub-sample of $-19 \sim -20$ gives a large Ω_m but still agrees with others within the error bars. The results of model B

shown in Table 6 are similar to those in Table 3. Here Ω_m from all the sub-samples are larger than 0.3, especially the one from the sub-sample of $-19 \sim -20$ which is unusually large at $0.73_{-0.27}^{+0.19}$. Meanwhile, the pairwise velocity variance estimated from the sub-sample of $-21 \sim -20$ has an extraordinary value of $1014.28_{-113.57}^{+51.42} \text{ km s}^{-1}$. These raise questions on the prior of $\sigma_8 = 0.74$.

Finally, we take σ_8 , b and σ_{pv} as fitting parameters, while fixing $\Omega_m = 0.24$. The best fitting parameters are given in Table 7. Again we have results similar to those listed in Table 4. All the values of σ_8 are always ≥ 0.8 , which suggests that the low σ_8 value is unlikely to match the 2dFGRS.

5.5 Fitting with Scale Dependent Bias

In the above fitting, we assumed scale-independent galaxy bias. Recently, there are pieces of evidence showing that galaxy bias is scale dependant, and the dependence is different for red and blue galaxies (Cole et al. 2005; Seo & Eisenstein 2005; Percival et al. 2007; Jeong & Komatsu 2006; Guzik et al. 2007; Smith et al. 2007; Huff et al. 2007). The scale dependence of the bias parameter would change the shape of galaxy DWT power spectrum, and could lead to misinterpretation of the matter content, Ω_m , if it is not properly taken into account. Therefore, we will show our fitting with a scale-dependent galaxy bias model.

We model the scale dependence bias from the estimation given by Cole et al. (2005) in figure 15 of their paper, which could be approximated as

$$b_k = b_0[1 + (k/0.1)^{0.1}]. \quad (15)$$

Combining with Equation (B12), we can obtain

$$b_j = b_0[1 + ((2^{j+1}\pi n_p)/0.1L)^{0.1}]. \quad (16)$$

Hence, $\beta_j = \Omega_m^{0.6}/b_j$. We incorporate the scale dependence bias model with Equation (7) and obtain

$$P_j^S = b_j^2(1 + \beta_j S_j)^2 S_j^{\text{PV}} P_j. \quad (17)$$

We then perform the fittings as in Section 5.2 with the above equation. The results are shown in Tables 8 and 9. The marginal PDFs are shown in Figures 9 and 10.

Lower values of Ω_m are now found in the results. This is because the value bias parameter keeps on increasing as j grows (or as the scale decreases). The scale dependent factor b_j will alter the shape the DWT power spectrum, making it decrease more slowly as j increases than when b was assumed scale independent.

Generally, fitting with scale-dependent bias parameters shows less differences between models with $\sigma_8 = 0.84$ and $\sigma_8 = 0.74$, but the differences are still there. For the value of Ω_m , fitting with $\sigma_8 = 0.74$ still gives central values as high as 0.38 and 0.39 for the two sub-samples, and these two values seem to be inconsistent with that given by the sub-sample $-20 \sim -21$ within $1 - \sigma$ error. While for the fitting results of $\sigma_8 = 0.84$, values of Ω_m from all the three sub-samples are consistent within the 1σ errors. Note also that the fitting results of $-20 \sim -21$ with different value of σ_8 are very close to each other, with $\Omega_m = 0.25_{-0.02}^{+0.02}$ for $\sigma_8 = 0.84$ and $\Omega_m = 0.23_{-0.02}^{+0.02}$. The fitting value of Ω_m from this sub-sample is consistent very well with that given by Cole et al. (2005).

6 CONCLUSIONS AND DISCUSSION

DWT power spectra of 2dFGRS samples are measured on scales equivalent to $0.035 < k < 2.2h \text{ Mpc}^{-1}$. We show that these power spectra are efficient for testing Λ CDM models with high and low amplitudes of mass density fluctuations. The model with $\sigma_8 = 0.84$ finds good support from the 2dFGRS sample, all the best fitting parameters, b , β , σ_{pv} , are consistent with the other works on 2dFGRS. Especially, three volume-limited samples gave different b and β values, but approximately the same values of $\Omega_m = (b\beta)^{1/0.6} = 0.28 - 0.36$. On the other hand, the model with $\sigma_8 = 0.74$ does not give such consistent fitting results, the best fitted Ω_m from the three volume-limited samples are significantly different, with above 1σ discrepancies, from ~ 0.3 upward. Moreover, the fitting results of σ_{pv} are generically large, even reach 10^3 km s^{-1} . Even when the scale dependence of the galaxy bias parameter is taken into account, differences still exist between the fitting results of the two models. Fitting with $\sigma_8 = 0.74$ still gives inconsistent values of Ω_m the for three sub-samples. Our studies suggest that the power spectrum of 2dFGRS disfavors models

with low amplitude of mass fluctuations, $\sigma_8 = 0.74$, if the other cosmological parameters are given by the WMAP3. For the fitting value of Ω_m to be consistent with that given by WMAP3, strong scale dependence of bias parameters is needed.

It is found that σ_{pv} increases with luminosity, which is basically consistent with the observation of Jing & Börner (2004) though our estimated values are lower than theirs.

Another parameter that will affect the shape of the DWT power spectrum is the slope of the primordial fluctuation spectrum n_s . We have been using the scale-invariant spectrum, or the Zeldovich spectrum with $n_s = 1$. However, we noticed that WMAP3 gives $n_s = 0.95^{+0.015}_{-0.019}$, which is 5% smaller. In order to check the influence of a lower value of n_s on our fitting results, we repeated our fitting for the sub-sample $-20 \sim -21$ with $n_s = 0.95$. We then found $b = 1.07^{+0.01}_{-0.01}$, $\beta = 0.44^{+0.02}_{-0.02}$ ($\Omega_m = 0.29^{+0.02}_{-0.02}$), and $\sigma_{\text{pv}} = 550^{+20}_{-20} \text{ km s}^{-1}$. Clearly, the change of n_s from 1 to 0.95 results in little modification to b and σ_{pv} , and only slightly alters (by less than 5%) the value of β , or Ω_m .

In this paper, we used only the diagonal modes in terms of \mathbf{j} , $P_{\mathbf{j}} = \langle \tilde{\epsilon}_{\mathbf{j}}, \mathbf{l} \tilde{\epsilon}_{\mathbf{j}}, \mathbf{l} \rangle$ and $\mathbf{j} = (j, j, j)$. Even in the second order statistics of the DWT, $\langle \tilde{\epsilon}_{\mathbf{j}}, \mathbf{l} \tilde{\epsilon}_{\mathbf{j}}, \mathbf{l}' \rangle$, we can have the power of the off-diagonal modes $P_{\mathbf{j}} = \langle \tilde{\epsilon}_{\mathbf{j}}, \mathbf{l} \tilde{\epsilon}_{\mathbf{j}}, \mathbf{l} \rangle$ and $\mathbf{j} = (j_1, j_2, j_3)$. In addition, we have the correlation between modes (\mathbf{j}, \mathbf{l}) and $(\mathbf{j}, \mathbf{l}')$ ($\mathbf{l} \neq \mathbf{l}'$). It has been shown that different parts of the second order statistics of DWT contain different information of the random field (Yang et al. 2001a). Possible constraints on the parameters given by various parts of the second order DWT statistics deserve further study.

Acknowledgements We thank the referee for helpful comments. We thank Shaun Cole, Carlton Baugh, Enzo Branchini, Steve Hatton, their Durham astrophysics theory group, and the VIRGO consortium for the Hubble Volume mock catalogs. The Virgo 256³ simulation we used in this paper was carried out by the Virgo Supercomputing Consortium using computers based at Computing Center of the Max-Planck Society at Garching and at the Edinburgh Parallel Computing Center. The data are publicly available at www.mpa-garching.mpg.de/NumCos. YCC and LLLF are supported by the NSFC under Grant 10373012, JP is supported by preliminary funding from PMO in the One-Hundred-Talent program of CAS and NSFC through Grant 10643002, and LZJ is supported by the US NSF under Grant AST-0507340.

Appendix A: DWT DECOMPOSITION OF RANDOM FIELD

For the details of the mathematical properties of the DWT, please refer to Mallat (1989a,b), Meyer (1992), Daubechies (1992), and for physical applications, refer to Fang & Thews (1998). For this application, the most important properties are 1) orthogonality, 2) completeness, and 3) locality in both scale (r) and physical position (x). Wavelets with compactly supported basis are an excellent means to analyze random fields. Among the compactly supported orthogonal wavelets, the Daubechies family of wavelets is easy to implement.

To simplify the notation, we consider a 1-D field $\rho(x)$ on spatial range L . It is straightforward to generalize to 3-D fields. In DWT analysis, the space L is chopped into 2^j segments labelled by $l = 0, 1, \dots, 2^j - 1$. Each of the segments has size $L/2^j$. The index j is a positive integer which represents scale $L/2^j$. The index l gives position and corresponds to spatial range $lL/2^j < x < (l+1)L/2^j$.

DWT analysis uses two functions, the scaling functions $\phi_{j,l}(x) = (2^j/L)^{1/2} \phi(2^j/L - l)$, and wavelets $\psi_{j,l}(x) = (2^j/L)^{1/2} \psi(2^j/L - l)$. The scaling functions and wavelets are given respectively by a translation and dilation of the basic scaling function $\phi(\eta)$ and basic wavelet $\psi(\eta)$ as

$$\phi_{j,l}(x) = \left(\frac{2^j}{L}\right)^{1/2} \phi(2^j x/L - l), \quad (\text{A.1})$$

and

$$\psi_{j,l}(x) = \left(\frac{2^j}{L}\right)^{1/2} \psi(2^j x/L - l). \quad (\text{A.2})$$

The scaling functions play the role of window function. They are used to calculate the mean field in the segment l . The wavelets $\psi_{j,l}(x)$ capture the difference between the mean fields at space ranges $lL/2^j < x < (l+1/2)L/2^j$ and $(l+1/2)L/2^j < x < (l+1)L/2^j$.

The scaling functions and wavelets $\psi_{j,l}(x)$ satisfy the orthogonal relations,

$$\int \phi_{j,l}(x)\phi_{j,l'}(x)dx = \delta_{l,l'}, \quad (\text{A.3})$$

$$\int \psi_{j,l}(x)\psi_{j',l'}(x)dx = \delta_{j,j'}\delta_{l,l'}, \quad (\text{A.4})$$

$$\int \phi_{j,l}(x)\psi_{j',l'}(x)dx = 0, \quad \text{if } j' \geq j. \quad (\text{A.5})$$

With these properties, a 1-D random field $\rho(x)$ can be decomposed into

$$\rho(x) = \rho^j(x) + \sum_{j'=j}^{\infty} \sum_{l=0}^{2^{j'}-1} \tilde{\epsilon}_{j',l}\psi_{j',l}(x), \quad (\text{A.6})$$

where

$$\rho^j(x) = \sum_{l=0}^{2^j-1} \epsilon_{j,l}\phi_{j,l}(x). \quad (\text{A.7})$$

The scaling function coefficient (SFC) $\epsilon_{j,l}$ and the wavelet function coefficient (WFC), $\tilde{\epsilon}_{j,l}$, are given by

$$\epsilon_{j,l} = \int \rho(x)\phi_{j,l}(x)dx, \quad (\text{A.8})$$

and

$$\tilde{\epsilon}_{j,l} = \int \rho(x)\psi_{j,l}(x)dx, \quad (\text{A.9})$$

respectively. The SFC $\epsilon_{j,l}$ measure the mean of $\rho(x)$ in the segment l , while the WFC $\tilde{\epsilon}_{j,l}$ measures the fluctuations (or difference) of field $\rho(x)$ at l on scale j .

The first term on the r.h.s. of Equation (A6), $\rho^j(x)$, is the field $\rho(x)$ smoothed on the scale j , while the second term contains all information on scales $\geq j$. Because of the orthogonality, the decomposition between the scales of $< j$ (first term) and $\geq j$ (second term) in Equation (A6) is unambiguous.

Appendix B: 1-D DWT POWER SPECTRUM

The contrast (or perturbation) of the field $\rho(x)$ is defined by

$$\delta(x) = \frac{\rho(x) - \bar{\rho}}{\bar{\rho}}, \quad (\text{B.1})$$

where $\bar{\rho}$ is the mean density of the field. The Fourier expansion of ϵ is

$$\delta(x) = \sum_{n=-\infty}^{\infty} \epsilon_n e^{i2\pi n x/L}, \quad (\text{B.2})$$

with the coefficients given by

$$\epsilon_n = \frac{1}{L} \int_0^L \delta(x) e^{-i2\pi n x/L} dx. \quad (\text{B.3})$$

Parseval's theorem relates the power for a distribution to the coefficients of the Fourier expansion. This yields

$$\frac{1}{L} \int_0^L |\epsilon(x)|^2 dx = \sum_{n=-\infty}^{\infty} |\epsilon_n|^2, \quad (\text{B.4})$$

which shows that the perturbations can be decomposed into domains, n , by the orthonormal Fourier basis functions. The power spectrum of perturbations on scale L/n is then defined as

$$P(n) = |\epsilon_n|^2. \quad (\text{B.5})$$

This is the power spectrum with respect to the Fourier decomposition.

Similarly Parseval's theorem for the DWT is

$$\frac{1}{L} \int_0^L |\epsilon(x)|^2 dx = \sum_{j=0}^{\infty} \frac{1}{L} \sum_{l=0}^{2^j-1} |\tilde{\epsilon}_{j,l}|^2. \quad (\text{B.6})$$

Thus, the second order statistical behavior of $\epsilon(x)$ can be described by the $|\tilde{\epsilon}_{j,l}|^2$ and one can call $|\tilde{\epsilon}_{j,l}|^2$ the DWT power spectrum.

Comparing Equations (B4) and (B6), it is clear that $\frac{1}{L} \sum_{l=0}^{2^j-1} |\tilde{\epsilon}_{j,l}|^2$ is a measure of the power of the perturbation on scales from $L/2^j$ to $L/2^{j+1}$. Therefore, the power spectrum with respect to the wavelet basis can be defined as

$$P_j = \frac{1}{2^j} \sum_{l=0}^{2^j-1} |\tilde{\epsilon}_{j,l}|^2. \quad (\text{B.7})$$

Since the DWT bases $\psi_{j,l}(x)$ measure the differences between the *local* mean densities at adjoining scales, the mean density on length scales larger than the sample size is not needed in calculating $\tilde{\epsilon}_{j,l}$. The spectrum Equation (B7) will not be affected by the infrared (long-wavelength) uncertainty of the mean density.

With Equations (B2), (B6), (A2) and (A4) we can find the relation between the power spectra of DWT P_j and Fourier $P(n)$. It is

$$P_j = \frac{1}{2^j} \sum_{n=-\infty}^{\infty} |\hat{\psi}(n/2^j)|^2 P(n), \quad (\text{B.8})$$

where $\hat{\psi}(n)$ is the Fourier transform of the basic wavelet given by

$$\hat{\psi}(n) = \int_0^L \psi(\eta) e^{-i2\pi n\eta} d\eta. \quad (\text{B.9})$$

Since wavelet is admissible, i.e. $\int \psi(\eta) d\eta = 0$, we have $\hat{\psi}(0) = 0$. $|\hat{\psi}(n)|^2$ is localized in n -space. $|\hat{\psi}(n)|^2$ has symmetrically distributed peaks with respect to $n = 0$. The first highest peaks are non-zero in two narrow ranges centered at $n = \pm n_p$ with width Δn_p . Besides the first peak, there are "side lobes" in $|\hat{\psi}(n)|^2$. However, the "side lobes" are small, for instance, for the Daubechies 4 wavelet, the area under the "side lobes" is not more than 2% of the first peak. Therefore, P_j is a good estimation of the band-averaged Fourier power spectrum centered at wavenumber

$$n_j = n_p 2^j. \quad (\text{B.10})$$

The band width is

$$\Delta n = 2^j \Delta n_p. \quad (\text{B.11})$$

In other words, the relation between k and j is

$$\log k = (\log 2)j - \log(L/2\pi) + \log n_p. \quad (\text{B.12})$$

For the D4 wavelet, $\log n_p = 0.270$.

Appendix C: 3-D DWT POWER SPECTRUM

For 3-D random field, the DWT decomposition is based on the orthogonal and complete set of 3-D wavelet basis, $\{\psi_{\mathbf{j}, \mathbf{l}}(\mathbf{x})\}$, which can be constructed by a direct product of 1-D wavelet basis as

$$\psi_{\mathbf{j}, \mathbf{l}}(\mathbf{x}) = \psi_{j_1, l_1}(x_1)\psi_{j_2, l_2}(x_2)\psi_{j_3, l_3}(x_3), \quad (\text{C.1})$$

where $j_i = 0, 1, 2, \dots$ ($i = 1, 2, 3$) and $l_i = 0 \dots 2^{j_i-1}$. Obviously, the basis $\psi_{\mathbf{j}, \mathbf{l}}(\mathbf{x})$ is non-zero mainly in a volume $L_1/2^{j_1} \times L_2/2^{j_2} \times L_3/2^{j_3}$, and around the position $(x_1 = l_1 L_1/2^{j_1}, x_2 = l_2 L_2/2^{j_2}, x_3 = l_3 L_3/2^{j_3})$ (Fang & Thews 1998). Similar to Equation (B7), the power spectrum on scale $\mathbf{j} = (j_1, j_2, j_3)$ is

$$P_{\mathbf{j}}^2 = \frac{1}{2^{j_1+j_2+j_3}} \sum_{l_1=0}^{2^{j_1-1}} \sum_{l_2=0}^{2^{j_2-1}} \sum_{l_3=0}^{2^{j_3-1}} [\tilde{\epsilon}_{\mathbf{j}, \mathbf{l}}]^2. \quad (\text{C.2})$$

For 3-D samples, Equation (B8) is generalized as

$$P_{\mathbf{j}} = \frac{1}{2^{j_1+j_2+j_3}} \sum_{n_1=-\infty}^{\infty} \sum_{n_2=-\infty}^{\infty} \sum_{n_3=-\infty}^{\infty} |\hat{\psi}(n_1/2^{j_1})\hat{\psi}(n_2/2^{j_2})\hat{\psi}(n_3/2^{j_3})|^2 P(n_1, n_2, n_3). \quad (\text{C.3})$$

Because the cosmic density field is isotropic, the Fourier power spectrum $P(n_1, n_2, n_3)$ is dependent only on

$$n = \sqrt{n_1^2 + n_2^2 + n_3^2}. \quad (\text{C.4})$$

Obviously, the DWT power spectrum is invariant with respect to the cyclic permutation of index as

$$P_{j_1, j_2, j_3} = P_{j_3, j_1, j_2} = P_{j_2, j_3, j_1}. \quad (\text{C.5})$$

Considering Equations (C3) and (C4), we can formally define a band center wavenumber $n_{\mathbf{j}}$ corresponding to the 3-D mode \mathbf{j} as

$$n_{\mathbf{j}} = n_p \sqrt{(2^{j_1})^2 + (2^{j_2})^2 + (2^{j_3})^2}. \quad (\text{C.6})$$

For an isotropic random field, the Fourier modes with the same n are statistically equivalent. However, the DWT modes with the same $n_{\mathbf{j}}$ [Eq. (C6)] are not statistically equivalent, because the DWT modes are not rotationally invariant. A Fourier mode $e^{-i(2\pi/L)(n_1 x_1 + n_2 x_2 + n_3 x_3)}$ can be obtained by a rotation of mode $e^{-i(2\pi/L)(n'_1 x_1 + n'_2 x_2 + n'_3 x_3)}$ as long as $n_1'^2 + n_2'^2 + n_3'^2 = n_1^2 + n_2^2 + n_3^2$. However, the DWT modes do not have the same property. Generally, one cannot transform a mode (j_1, j_2, j_3) to (j'_1, j'_2, j'_3) by a rotation, even when $n_{\mathbf{j}} \simeq n_{\mathbf{j}'}$. Because of different configurations between them, the condition $n_{\mathbf{j}} n_{\mathbf{j}'}$ generally does not imply

$$P_{\mathbf{j}} = P_{\mathbf{j}'}. \quad (\text{C.7})$$

This invariance holds only when (j_1, j_2, j_3) is a cyclic permutation of (j'_1, j'_2, j'_3) .

With this property, one can define two types of the DWT power spectra: 1) The diagonal power spectrum given by $P_{\mathbf{j}}$ on diagonal modes $j_1 = j_2 = j_3 = j$, and 2) Off-diagonal power spectrum given by other modes.

From Equation (C3), the diagonal power spectrum $P_{\mathbf{j}} \equiv P_{j, j, j}$ is related to the Fourier power spectrum by

$$P_{\mathbf{j}} = \sum_{n_1=-\infty}^{\infty} \sum_{n_2=-\infty}^{\infty} \sum_{n_3=-\infty}^{\infty} W_{\mathbf{j}}(n_1, n_2, n_3) P(n_1, n_2, n_3), \quad (\text{C.8})$$

where the window function $W_{\mathbf{j}}$ is

$$W_{\mathbf{j}}(n_1, n_2, n_3) = \frac{1}{2^{3j}} |\hat{\psi}(n_1/2^j)\hat{\psi}(n_2/2^j)\hat{\psi}(n_3/2^j)|^2, \quad (\text{C.9})$$

with the normalization

$$\int_{-\infty}^{\infty} W_j(n_1, n_2, n_3) dn_1 dn_2 dn_3 = 1. \quad (\text{C.10})$$

The window function W_j is localized around $n_1 = n_2 = n_3 = n_p 2^j$. Therefore, the diagonal power spectrum P_j is a band-average of the isotropic Fourier power spectrum $P(n)$ with the central frequency $n = \sqrt{3} n_g 2^j$.

There are two types of modes: diagonal mode with $j_1 = j_2 = j_3$; off-diagonal mode for which the three numbers (j_1, j_2, j_3) are not the same. The DWT estimator can provide two types of power spectra: 1) Diagonal power spectrum given by the powers on diagonal modes, 2) Off-diagonal power spectrum given by the powers on off-diagonal modes. Because the two types of modes have different spatial invariance, the diagonal and off-diagonal DWT power spectra are very flexible to deal with configuration-related problems in the power spectrum detection. For off-diagonal modes, one can also calculate the linear non-diagonal DWT power spectrum P_{j_1, j_2, j_3} via Equation (C2). However, in this case, P_{j_1, j_2, j_3} cannot simply be identified as a band average of the isotropic Fourier power spectrum $P(n)$ centered at $n = n_j$. Nevertheless, n_j is useful to calibrate the physical scale of a given j .

Appendix D: REDSHIFT SPACE DWT POWER SPECTRUM

Unlike FFT power spectrum algorithm for redshift distortion, which is empirical, DWT power spectrum estimator has more strict algorithm which was introduced by (Yang et al. 2002).

The position of galaxy i in redshift space is given by $\mathbf{s}_i = \mathbf{x}_i + \hat{\mathbf{r}} v_r(\mathbf{x}_i)/H_0$, where v_r is the radial component of $\mathbf{v}(\mathbf{x})$ and $\mathbf{v}(\mathbf{x})$ the mean galaxy velocity at \mathbf{x} . The number density distribution in redshift space is then

$$n^S(\mathbf{s}) = \sum_{i=1}^{N_g} w_i \delta_D[\mathbf{s} - \mathbf{x}_i - \hat{\mathbf{r}} v_r(\mathbf{x}_i)/H_0] = \bar{n}^S(\mathbf{s})[1 + \delta^S(\mathbf{s})], \quad (\text{D.1})$$

where $\bar{n}^S(\mathbf{s})$ is the selection function in redshift space. The power spectrum in redshift space can be given as

$$P_{\mathbf{j}}^S = \frac{1}{2^{j_1+j_2+j_3}} \sum_{l_1=0}^{2^{j_1}-1} \sum_{l_2=0}^{2^{j_2}-1} \sum_{l_3=0}^{2^{j_3}-1} [\tilde{\epsilon}_{\mathbf{j}, \mathbf{l}}^S]^2 - \frac{1}{2^{j_1+j_2+j_3}} \sum_{l_1=0}^{2^{j_1}-1} \sum_{l_2=0}^{2^{j_2}-1} \sum_{l_3=0}^{2^{j_3}-1} \int \frac{\psi_{\mathbf{j}, \mathbf{l}}^2(\mathbf{x})}{\bar{n}^S(\mathbf{x})} d\mathbf{x}, \quad (\text{D.2})$$

where

$$\tilde{\epsilon}_{\mathbf{j}, \mathbf{l}}^S = \int \frac{n^S(\mathbf{s})}{\bar{n}^S(\mathbf{s})} \psi_{\mathbf{j}, \mathbf{l}}(\mathbf{s}) d\mathbf{s}. \quad (\text{D.3})$$

Using an auxiliary vector \mathbf{J} , and taking ensemble average of velocity, we can obtain from Equations (D1) and (D3),

$$\langle \tilde{\epsilon}_{\mathbf{j}, \mathbf{l}}^S \rangle_v = \sum_{i=1}^{N_g} w_i \int d\mathbf{s} \delta_D(\mathbf{s} - \mathbf{x}_i + i\nabla_{\mathbf{J}}) \cdot e^{i\mathbf{J} \cdot \hat{\mathbf{r}} v_r(\mathbf{x}_i)/H_0 - (1/2)\sigma_{pv}^2(\mathbf{x}_i)(\mathbf{J} \cdot \hat{\mathbf{r}})^2 H_0^2} \psi_{\mathbf{j}, \mathbf{l}}(\mathbf{s})|_{\mathbf{J}=0}, \quad (\text{D.4})$$

where the the velocity field is assumed to be *Gaussian*, $\sigma_{pv}^2(\mathbf{x}) = \langle [v_i(\mathbf{x}) - V_i(\mathbf{x})]^2 \rangle_v$ is the *rms* deviation of velocity $\mathbf{v}(\mathbf{x})$. If we consider only linear effect of the bulk velocity, we have

$$\delta(\mathbf{x}) = -\frac{1}{H_0\beta} \nabla \cdot \mathbf{V}(\mathbf{x}), \quad (\text{D.5})$$

where $\beta \simeq \Omega_m^{0.6}/b$ is the redshift distortion parameter. Then, Equation (D4) can be written as

$$\langle \tilde{\epsilon}_{\mathbf{j}, \mathbf{l}}^S \rangle_v = \sum_{i=1}^{N_g} w_i \int d\mathbf{s} \psi_{\mathbf{j}, \mathbf{l}}(\mathbf{s}) e^{-(1/2)\sigma_{pv}^2(\mathbf{s})(\hat{\mathbf{r}} \cdot \nabla)^2} \delta_D(\mathbf{s} - \mathbf{x}_i) - \frac{1}{H_0} \sum_{i=1}^{N_g} w_i \int d\mathbf{s} \hat{\mathbf{r}} \cdot [\nabla_s v_r(\mathbf{s} + i\nabla_{\mathbf{J}}) \delta_D(\mathbf{s} - \mathbf{x}_i + i\nabla_{\mathbf{J}})] e^{-(1/2)\sigma_{pv}^2(\mathbf{x}_i)(\mathbf{J} \cdot \hat{\mathbf{r}})^2} \psi_{\mathbf{j}, \mathbf{l}}(\mathbf{s})|_{\mathbf{J}=0}. \quad (\text{D.6})$$

Neglecting terms of the order $V_r(\mathbf{x})\delta(\mathbf{x})$, and using the linear relation Equation (D5), Equation (D6) gives

$$\langle \tilde{\epsilon}_{\mathbf{j}, \mathbf{l}}^S \rangle_v = \int d\mathbf{s} \psi_{\mathbf{j}, \mathbf{l}}(\mathbf{s}) e^{(1/2)\sigma_{\text{pv}}^2(\mathbf{s})(\hat{\mathbf{r}} \cdot \nabla)^2} n^g(\mathbf{s}) + \beta \int d\mathbf{s} \psi_{\mathbf{j}, \mathbf{l}}(\mathbf{s}) (\hat{\mathbf{r}} \cdot \nabla_s)^2 \nabla^{-2} e^{-(1/2)\sigma_{\text{pv}}^2(\mathbf{s})(\hat{\mathbf{r}} \cdot \nabla)^2} n^g(\mathbf{s}). \quad (\text{D.7})$$

Because all operators in the integrand of Equation (D7) are nearly diagonal in the DWT representation (Farge et al. 1996), Equation (D7) can be rewritten as

$$\tilde{\epsilon}_{\mathbf{j}, \mathbf{l}}^S = (1 + \beta S_{\mathbf{j}}) s_{\mathbf{j}}^{\text{PV}} \tilde{\epsilon}_{\mathbf{j}, \mathbf{l}}, \quad (\text{D.8})$$

where

$$S_{\mathbf{j}} = \int \psi_{\mathbf{j}, \mathbf{l}}(\mathbf{x}) (\hat{\mathbf{r}} \cdot \nabla)^2 \nabla^{-2} \psi_{\mathbf{j}, \mathbf{l}}(\mathbf{x}) d\mathbf{x}, \quad (\text{D.9})$$

and

$$s_{\mathbf{j}}^{\text{PV}} = \int \psi_{\mathbf{j}, \mathbf{l}}(\mathbf{x}) e^{(1/2)\sigma_{\text{pv}}^2(\mathbf{x})(\hat{\mathbf{r}} \cdot \nabla)^2} \psi_{\mathbf{j}, \mathbf{l}}(\mathbf{x}) d\mathbf{x}. \quad (\text{D.10})$$

Substituting equation Equation (D8) into Equation (D2), we have the redshift distorted power spectrum as

$$P_{\mathbf{j}}^S = (1 + \beta S_{\mathbf{j}})^2 S_{\mathbf{j}}^{\text{PV}} P_{\mathbf{j}}, \quad (\text{D.11})$$

where $S_{\mathbf{j}}^{\text{PV}} = [s_{\mathbf{j}}^{\text{PV}}]^2 (1 + \beta S_{\mathbf{j}})^2$ is the linear redshift distortion factor, and $S_{\mathbf{j}}^{\text{PV}}$ the non-linear redshift distortion factor due to pairwise velocity dispersion.

For plane-parallel approximation, if we take coordinate x_3 as the line-of-sight direction, the linear redshift distortion $S_{\mathbf{j}}$ is

$$S_{\mathbf{j}} = \int \psi_{\mathbf{j}, \mathbf{l}}(\mathbf{x}) \frac{\partial^2}{\partial x_3^2} \nabla^{-2} \psi_{\mathbf{j}, \mathbf{l}}(\mathbf{x}) d\mathbf{x}. \quad (\text{D.12})$$

The Fourier transform of $\psi_{\mathbf{j}, \mathbf{l}}$ is

$$\psi_{\mathbf{j}, \mathbf{l}} = \frac{1}{L} \sum_{n=-\infty}^{\infty} \hat{\psi}_{\mathbf{j}, \mathbf{l}}(n) e^{-i2\pi n x/L}, \quad (\text{D.13})$$

and

$$\hat{\psi}_{\mathbf{j}, \mathbf{l}}(n) = \left(\frac{L}{2^j}\right)^{1/2} \hat{\psi}(n/2^j) e^{-i2\pi n l/2^j}, \quad (\text{D.14})$$

where $\hat{\psi}(n)$ is the Fourier transform of the basic wavelet,

$$\hat{\psi}(n) = \int_{-\infty}^{\infty} \psi(\eta) e^{-i2\pi n \eta} d\eta. \quad (\text{D.15})$$

Equation (D12) can now be written as

$$S_{j_1, j_2, j_3} = \frac{1}{2^{j_1+j_2+j_3}} \sum_{n_1, n_2, n_3=-\infty}^{\infty} \frac{(n_3/L_3)^2}{(n_1/L_1)^2 + (n_2/L_2)^2 + (n_3/L_3)^2} |\hat{\psi}(n_1/2^{j_1}) \hat{\psi}(n_2/2^{j_2}) \hat{\psi}(n_3/2^{j_3})|^2. \quad (\text{D.16})$$

For $\sigma_v(\mathbf{x})$, we assume that it is independent of \mathbf{x} , then we have

$$s_{j_1, j_2, j_3}^{\text{PV}} = \frac{1}{2^{j_1+j_2+j_3}} \sum_{n_1, n_2, n_3=-\infty}^{\infty} |\hat{\psi}(n_1/2^{j_1}) \hat{\psi}(n_2/2^{j_2}) \hat{\psi}(n_3/2^{j_3})|^2 \exp[-(1/2)\sigma_{\text{pv}}^2(\hat{\mathbf{r}} \cdot \mathbf{n})^2], \quad (\text{D.17})$$

where $\mathbf{n} = 2\pi(n_1/L_1, n_2/L_2, n_3/L_3)$. If we further assume plane-parallel approximation, we have

$$s_{j_1, j_2, j_3}^{\text{PV}} = \frac{1}{2^{j_3}} \sum_{n_3=-\infty}^{\infty} |\hat{\psi}(n_3/2^{j_3})|^2 \exp[-(1/2)\sigma_{\text{pv}}^2(2\pi n_3/L_3)^2]. \quad (\text{D.18})$$

References

- Bacon D. J., Massey R. J., Refregier A. R. et al., 2003, MNRAS, 344, 673
- Bahcall N. A., Bode P., 2003, ApJ, 588, L1
- Cole S., Percival W. J., Peacock J. A. et al., 2005, MNRAS, 362, 505
- Cole S., Hatton S., Weinberg D. H. et al., 1998, MNRAS, 300, 945
- Colless M., Dalton G., Maddox S. et al., 2001, MNRAS, 328, 1039
- Colless M., Peterson B. A., Jackson C. et al., 2003, VizieR Online Data Catalog, 7226, 0
- Daubechies I., 1992, Ten Lectures on Wavelets. Philadelphia, SIAM
- Fang L.-Z., Feng L.-L., 2000, ApJ, 539, 5
- Fang L.-Z., Thews R., 1998, Wavelet in Physics. World Scientific, Singapore.
- Guzik J., Bernstein G., Smith R. E., 2006, ArXiv Astrophysics e-prints
- Hawkins E., Maddox S., Cole S. et al., 2003, MNRAS, 346, 78
- Hoekstra H., Yee H. K. C., Gladders M. D., 2002, ApJ, 577, 595
- Huff E., Schulz A. E., White M. et al., 2007, Astropart.Phys., 26, 351
- Jeong D., Komatsu E., 2006, ApJ, 651, 619
- Jing Y. P., Börner G., 2004, ApJ, 617, 782
- Mallat S. G., 1989a, IEEE Trans, on PAMI, 11, 674
- Mallat S. G., 1989b, Trans. Am. Math. Soc., 315, 69
- Meyer Y., 1992, Wavelets and Operators. Cambridge Press, New York.
- Norberg P., Baugh C. M., Hawkins E. et al., 2001, MNRAS, 328, 64
- Norberg P., Cole S., Baugh C. M. et al., 2002, MNRAS, 336, 907
- Pan J., Szapudi I., 2005, MNRAS, 362, 1363
- Pando J., Fang L.-Z., 1995, Bulletin of the American Astronomical Society, 27, 1411
- Pando J., Fang L.-Z., 1996, ApJ, 459, 1
- Peacock J. A., Dodds S. J., 1994, MNRAS, 267, 1020
- Peacock J. A., Cole S., Norberg P. et al., 2001, Nature, 410, 169
- Percival W. J., Baugh C. M., Bland-Hawthorn J. et al., 2001, MNRAS, 327, 1297
- Percival W. J., Burke D., Heavens A. et al., 2004, MNRAS, 353, 1201
- Percival W. J., Nichol R. C., Eisenstein D. J. et al., 2007, ApJ, 657, 645
- Refregier A., Rhodes J., Groth E. J., 2002, ApJ, 572, L131
- Reiprich T. H., Böhringer H., 2002, ApJ, 567, 716
- Seljak U., Makarov A., McDonald P. et al., 2005, Phys. Rev. D, 71, 103515
- Seo H.-J., Eisenstein D. J., 2005, ApJ, 633, 575
- Smith R. E., Peacock J. A., Jenkins A. et al., 2003, MNRAS, 341, 1311
- Smith R. E., Scoccimarro R., Sheth R. K., 2007, Phys. Rev. D, 75, 063512
- Spergel D. N., Bean R., Nolta M. R. et al., 2007, ApJS, 170, 377
- Tegmark M., Strauss M. A., Blanton M. R. et al., 2004, Phys. Rev. D, 69, 103501
- Tegmark M., Hamilton A. J. S., Xu Y., 2002, MNRAS, 335, 887
- Van Waerbeke L., Mellier Y., Pelló R. et al., 2002, A&A, 393, 369
- Viel M., Haehnelt M. G. 2006, MNRAS, 365, 231
- Yang X., Feng L., Chu Y., 2001, Progress in Astronomy, 19, 37
- Yang X., Feng L.-L., Chu Y. et al., 2001a, ApJ, 553, 1
- Yang X., Feng L.-L., Chu Y. et al., 2001b, ApJ, 560, 549
- Yang X., Feng L.-L., Chu Y. et al., 2002, ApJ, 566, 630
- Zhan H., Fang L.-Z., 2003, ApJ, 585, 12